The Astrophysical Journal, 814:144 (6pp), 2015 December 1 doi:10.1088/0004-637X/814/2/144

DEEP MULTI-TELESCOPE PHOTOMETRY OF NGC 5466. II. THE RADIAL BEHAVIOR OF THE MASS FUNCTION SLOPE*

G. Beccari[1], E. Dalessandro[2], B. Lanzoni[2], F. R. Ferraro[2], M. Bellazzini[3], and A. Sollima[3]
[1] European Southern Observatory, Karl–Schwarzschild-Strasse 2, D-85748 Garching bei München, Germany; gbeccari@eso.org
[2] Dipartimento di Fisica e Astronomia, Università degli Studi di Bologna, viale Berti Pichat 6/2, I-40127 Bologna, Italy
[3] INAF—Osservatorio Astronomico di Bologna, via Ranzani 1, I-40127 Bologna, Italy
Received 2015 October 5; accepted 2015 October 27; published 2015 November 30

ABSTRACT

We use a combination of data acquired with the Advanced Camera for Survey on board the *Hubble Space Telescope* and the Large Binocular Camera (LBC-blue) mounted on the Large Binocular Telescope to sample the main sequence (MS) stars of the globular cluster (GC) NGC 5466 in the mass range $0.3 < M/M_{\odot} < 0.8$. We derive the cluster's Luminosity Function (LF) in several radial regions, from the center of the cluster out to the tidal radius. After corrections for incompleteness and field contamination, this was compared to theoretical LFs, obtained by multiplying a simple power-law mass function in the form $dN/dm \propto m^{\alpha}$ by the derivative of the mass–luminosity relationship of the best-fit isochrone. We find that α varies from -0.6 in the core region to -1.9 in the outer region. This fact allows us to prove by observation that the stars in NGC 5466 have experienced the effects of mass segregation. We compare the radial variation of α from the center out to 5 core radii (r_c) in NGC 5466 and the GC M10, finding that the gradient of α in the first $5r_c$ is more than a factor of 2 shallower in NGC 5466 than in M10, in line with the differences in the clusters' relaxation timescales. NGC 5466 is dynamically younger than M10, with two-body relaxation processes only recently starting to shape the distribution of MS stars. This result fully agrees with the conclusion obtained in our previous works on the radial distribution of blue straggler stars, further confirming that this can be used as an efficient clock to measure the dynamical age of stellar systems.

Key words: binaries: general – globular clusters: general – globular clusters: individual (NGC 5466) – stars: luminosity function, mass function

1. INTRODUCTION

Globular Clusters (GCs) are among the most fascinating and intensively studied objects in the Galaxy. They are typically populated by millions of stars, whose age, distance, and chemical abundance are well known, thus making GCs the ideal benchmark to study stellar and dynamical evolution and to understand how these two apparently independent evolutionary channels can influence each other.

While the main engine of stellar evolution is stellar thermonuclear reactions, the long-term dynamical evolution of GCs is driven by two-body relaxation. The typical timescale in which two-body processes take place in stellar systems depends on their masses and radii (Spitzer 1987) and for GCs it is typically significantly shorter (1–2 Gyr; Meylan & Heggie 1997) than their age. Therefore GCs may have experienced basically all phases of dynamical evolution. Indeed they survive the early and violent expansion triggered by primordial gas expulsion and mass loss due to stellar evolution, then they evolve toward higher central densities, eventually reaching core collapse while losing stars through the boundary set by the tidal field of their host galaxy (Heggie & Hut 2003).

Because of two-body relaxation, heavier objects tend to sink toward the cluster centers (mass segregation), while less massive stars are forced toward more external orbits. Hence, one possible observational approach to trace the dynamical state of star clusters is to look at the radial variations of the luminosity function (LF) and/or mass function (MF) of main sequence (MS) stars (see, e.g., Da Costa 1982; Marconi et al. 2001; Albrow et al. 2002; Koch et al. 2004; De Marchi et al. 2007). This method only allows us to look for the effect of mass segregation in a range of masses between $\sim 0.8\,M_{\odot}$ (the present-day mass of stars located at the MS turn-off point of GCs) down to the mass corresponding to the limiting magnitude of observational data. Because of the effect of mass segregation, the slope α of the MF is expected to become steeper as the distance from the cluster center increases (e.g., Rood et al. 1999; Lee et al. 2003, 2004; Andreuzzi et al. 2004). For example, in Beccari et al. (2010) we studied the radial distribution of the MF slope in M10. We found α dropping from 0.7 in the center to -0.9 in the external regions. Supported by *N*-body simulations, we interpreted this radial change of the MF slope as a clear sign of mass segregation in M10. The obvious weakness in this approach is the need for very deep and accurate photometric measurement, even in the very central regions of the clusters where stellar densities seriously challenge the spatial resolution capabilities even of space-based observations.

Similarly, internal dynamics can be probed by means of massive "test particles" like Blue Straggler Stars (BSSs), binaries, and millisecond pulsars (Guhathakurta et al. 1998; Ferraro et al. 2001, 2003; Dieball et al. 2005; Heinke et al. 2006). Among them BSSs have been widely used for this purpose since they are relatively bright (and hence easily observable) and they are a typical population of any GC. Ferraro et al. (2012) have shown that the BSS radial distribution can be efficiently used to rank clusters according

* Based on data acquired using the Large Binocular Telescope (LBT). The LBT is an international collaboration among institutions in the United States, Italy and Germany. LBT Corporation partners are: The University of Arizona on behalf of the Arizona university system; Istituto Nazionale di Astrofisica, Italy; LBT Beteiligungsgesellschaft, Germany, representing the Max-Planck Society, the Astrophysical Institute Potsdam, and Heidelberg University; The Ohio State University, and The Research Corporation, on behalf of The University of Notre Dame, University of Minnesota, and University of Virginia.

to their dynamical age and defined an empirical tool ("the dynamical clock") able to extract information about the dynamical state of GCs on the basis of only the position of the observed minimum in the BSS radial distribution. Three families have been identified in this way. *Family I* clusters are dynamically young, not showing significant signs of mass segregation, and having a flat BSS radial distribution (when properly compared to normal stars or to the sampled light). On the contrary, *Family II* and *Family III* GCs are classified as dynamically intermediate and old, as they show bimodal and monotonically decreasing BSS radial distributions, respectively. As expected, the large majority of the GCs studied so far are in a dynamically evolved state, with only a few notable exceptions (ω Centauri, NGC 2419, Palomar 14, NGC 6101, Arp 2, and Terzan 8; Ferraro et al. 2006; Dalessandro et al. 2008, 2015; Beccari et al. 2011; Salinas et al. 2012). In general a good agreement has been found among different indicators (see for example Beccari et al. 2006, 2013 for the cases of M62 and NGC 5466, respectively; Dalessandro et al. 2008 and Bellazzini et al. 2012 for NGC 2419). In particular, we have recently performed a detailed analysis of the dynamical state of NGC 6101 (Dalessandro et al. 2015), studying three different dynamical indicators (the BSS and the binary radial distributions and the radial variation of the LF and MF), and we consistently found a significant lack of mass segregation in this system. Opposite results from different indicators are obtained instead for the case of Palomar 14. In fact, based on the analysis of the radial distribution of BSSs Beccari et al. (2011) concluded that this cluster is not relaxed yet, while Frank et al. (2014) revealed a non-negligible variation of the MF slope across the cluster's inner regions. This apparent discrepancy between the two results can be reconciled with the hypothesis that the cluster was either primordially mass segregated and/or used to be significantly more compact in the past (Frank et al. 2014). Palomar 14 is one of the most remote GC in the Galaxy ($d \sim 66$ kpc), which makes it very hard to sample the MS at masses below $0.5\,M_{\odot}$ even with 8 m class telescopes. This fact once more suggests that the BSSs are a privileged sample of test particles to study the cluster's dynamics being these massive stars more than 6 mag brighter with respect to the low-mass end of the MS.

In Beccari et al. (2013, hereafter Paper I) we studied the BSS population of the Galactic GC NGC 5466, finding that it shows a bimodal radial distribution with a mild central peak and a minimum located at only $\sim 2.5 r_c$, where $r_c = 72''$ is the cluster's core radius (Miocchi et al. 2013). In the framework of the "dynamical clock" (Ferraro et al. 2012), we interpreted this feature in terms of a relatively young dynamical age. Interestingly, we also found that the radial distribution of binary stars seems to display a bimodal behavior, with the position of the minimum consistent with that of BSSs. In this paper we present the first analysis of the LF and MF along the entire radial extension of NGC 5466, obtained by combining deep high-resolution *Hubble Space Telescope* (*HST*) observations and ground-based Large Binocular Telescope (LBT) data. We compare these new results with those obtained in Paper I and we discuss their implication for our understanding of the dynamical state of this system. The paper is structured as follows: in Section 2 we describe the observations and data-analysis procedure, in Section 3 we derive the LF and the slope of the MF of NGC 5466 at different distances from the cluster center, and in Section 4 we discuss the obtained results in the framework of the dynamical evolution of the cluster.

Table 1
Log of the observations

Data Set	Number of Exposures	Filter	Exposure Time (s)	Date of Observations
		Deep Sample		
LBC-blue	11	*B*	400	2010 Apr 11
	15	*V*	200	2010 Apr 11
ACS	5	V_{606}	340	2006 Apr 12
	5	I_{814}	350	2006 Apr 12

2. CATALOGS AND PHOTOMETRIC COMPLETENESS

This work is based on the combination of deep high-resolution observations obtained with the *HST* Advanced Camera for Survey (ACS) and wide-field images acquired with the Large Binocular Camera (LBC) mounted at the LBT. The adopted reduction procedures are described in Paper I, where the photometric data set used here is referred as the "Deep Sample" (see also Table 1).

Briefly, we used the ACS images to sample the cluster MS in the *F*606*W* and *F*814*W* bands from the turn-off ($V \sim 20.5$) down to $V \sim 27$, in the first $\sim 120''$ from the cluster center. The deep LBC data allowed us to obtain a photometric catalog in the *B* and *V* bands sampling the MS down to comparable magnitudes in an area extending out to the cluster's tidal radius ($r_t = 1580''$; Miocchi et al. 2013). In Figure 1 we show the position of the field of view (FOV) of the *HST* and the LBT data sets with respect to the cluster center derived in Paper I.

The data reduction of the whole data set was performed through a standard point-spread function fitting procedure by using DAOPHOTII/ALLSTAR (Stetson 1987, 1994). We independently calibrated the ACS instrumental magnitudes into the VEGAMAG system adopting the standard procedure described in Sirianni et al. (2005).[4] We transformed the instrumental *B* and *V* magnitudes of the LBC sample into the Johnson/Kron-Cousins standard system by means of more than 200 stars in common with a photometric catalog previously published by Fekadu et al. (2007). Finally, the *F*606*W* filter was transformed into the Johnson *V* magnitude using the stars in common between the ACS and the LBC catalogs. This provides us with a homogenous V-magnitude scale in common between the two data sets.

In Figure 2 we show the color–magnitude diagrams (CMDs) obtained with the ACS and the LBC photometric catalogs (left and right panels, respectively). As already discussed in Paper I, a narrow MS is very well defined in both data sets, bearing witness to the exquisite quality of the ground-based images with respect to the ACS ones. The MS mean ridge lines for the two data sets are also shown (gray solid lines). In the same figure we also indicate the range of stellar masses sampled by our photometry. The transformation of the observed *V* magnitudes into solar masses is done by adopting the mass-to-light law of MS stars from the the best-fit isochrone of metallicity [Fe/H] $= -2.22$ and [α/Fe] $= 0.2$ from Dotter

[4] We used the newly zero points values which are available at the STScI web pages: http://www.stsci.edu/hst/acs/analysis/zeropoints

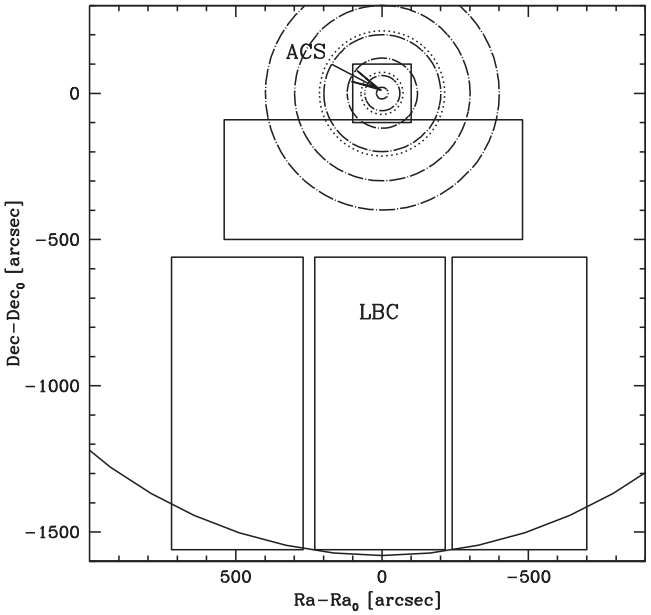

Figure 1. Map of the combined FOV of the data sets used to study the LF of NGC 5466 (this also corresponds to the "Deep Sample" used to study the cluster BSS and binary fractions in Paper I). The solid square corresponds to the ACS FOV, while the four rectangles mark the FOV of the LBC sample. The two dotted circles indicate the position of the core and half-mass radii ($r_c = 72''$ and $r_h = 214''$, respectively), while the large solid circle indicates the location of the cluster's tidal radius ($r_t = 1580''$). The cluster center is taken from Paper I and physical parameters are derived from Miocchi et al. (2013). The dash–dotted circles mark the radial regions considered in the present study for the analysis of the cluster LF, with the last annulus extending out to the tidal radius.

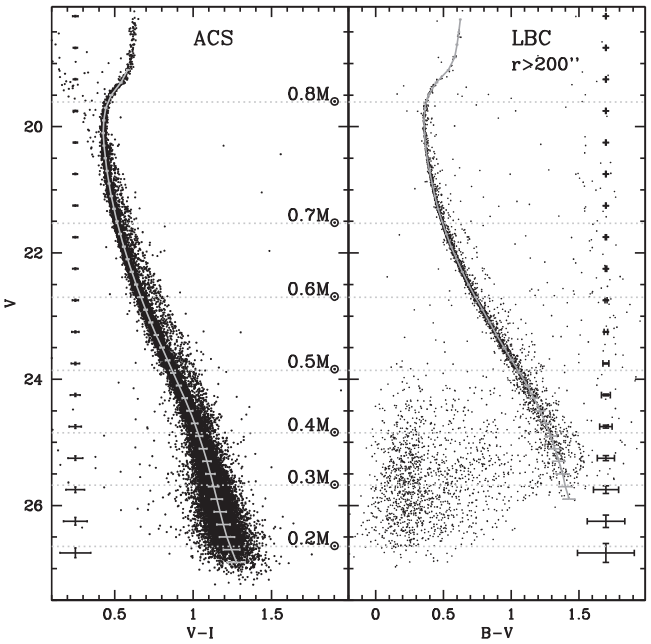

Figure 2. CMDs of the ACS and the LBC samples (left and right panels, respectively). The mean ridge line is shown as a solid gray line and its 1σ color uncertainty is also marked at different magnitude levels. The typical photometric errors (magnitudes and colors) for the two samples are indicated by black crosses. The conversion of the V magnitude into stellar masses is done using the mass-to-light law from the best-fit isochrone from Dotter et al. (2007).

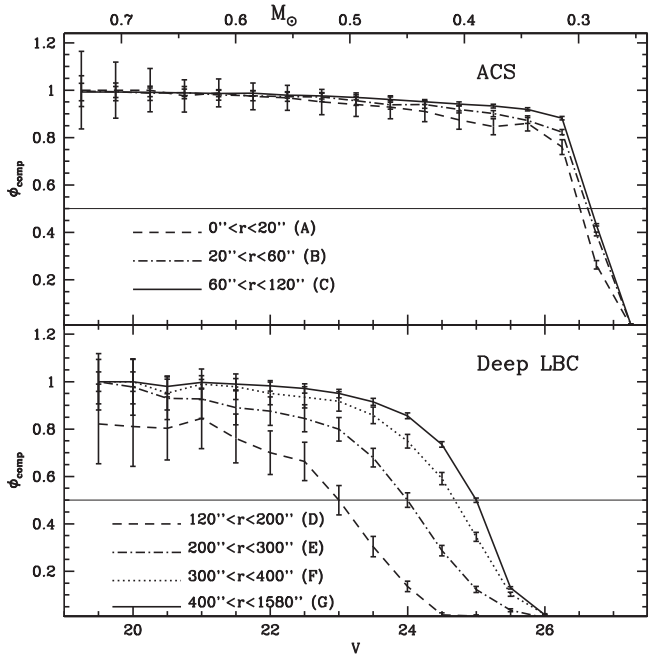

Figure 3. Photometric completeness ϕ as a function of the V magnitude for the ACS and the LBC data sets divided into three and four concentric radial areas, respectively. The solid horizontal line shows the limit of 50% of completeness. Since region D is characterized by a low completeness level all over the MS magnitude range, it has not been further considered for the LF analysis.

et al. (2007), and assuming a distance modulus $(m - M)_V = 16.16$ and a reddening $E(B - V) = 0.0$ from Ferraro et al. (1999). The same model was already used in Paper I to study the radial distribution of the BSS and binary fractions in NGC 5466.

The photometric completeness of the data set is evaluated through the use of artificial star experiments already described in Paper I. In short, following the recipe from Bellazzini et al. (2002), a number of artificial stars with V and I, or V and B magnitudes (depending on the data set) were randomly extracted from the observed LFs and spatially added to the science frame in a grid of cells of fixed width (five times larger than the typical full width at half maximum of the stars) in order to not introduce extra stellar crowding from the simulated stars on the images. Once the artificial stars are added to the images, the photometric reduction is repeated following the same strategy adopted for the original science frames. In particular, we extracted from the catalog of artificial stars the objects located inside a 2.5σ selection box from the MS mean ridge line. This sigma-clipping selection will be later done on the catalog of real stars to extract bona fide MS stars to be used to estimate the cluster's LF (see Section 3). Finally, the completeness is defined as the ratio between the number of simulated and recovered stars in a given magnitude bin within the range $19 < V < 27$ and a radial distance $0'' < r < 1600''$ from the cluster center.

In Figure 3 we show the photometric completeness (ϕ_{comp}) of the ACS and LBC data sets (upper and lower panels, respectively) in seven radial regions. The ACS data allow us to sample the MS with a 50% completeness ($\phi_{comp} = 0.5$) down to $V \sim 27$, corresponding to a stellar mass of $\sim 0.25\ M_\odot$. The seeing-limited ground-based images are obviously more affected

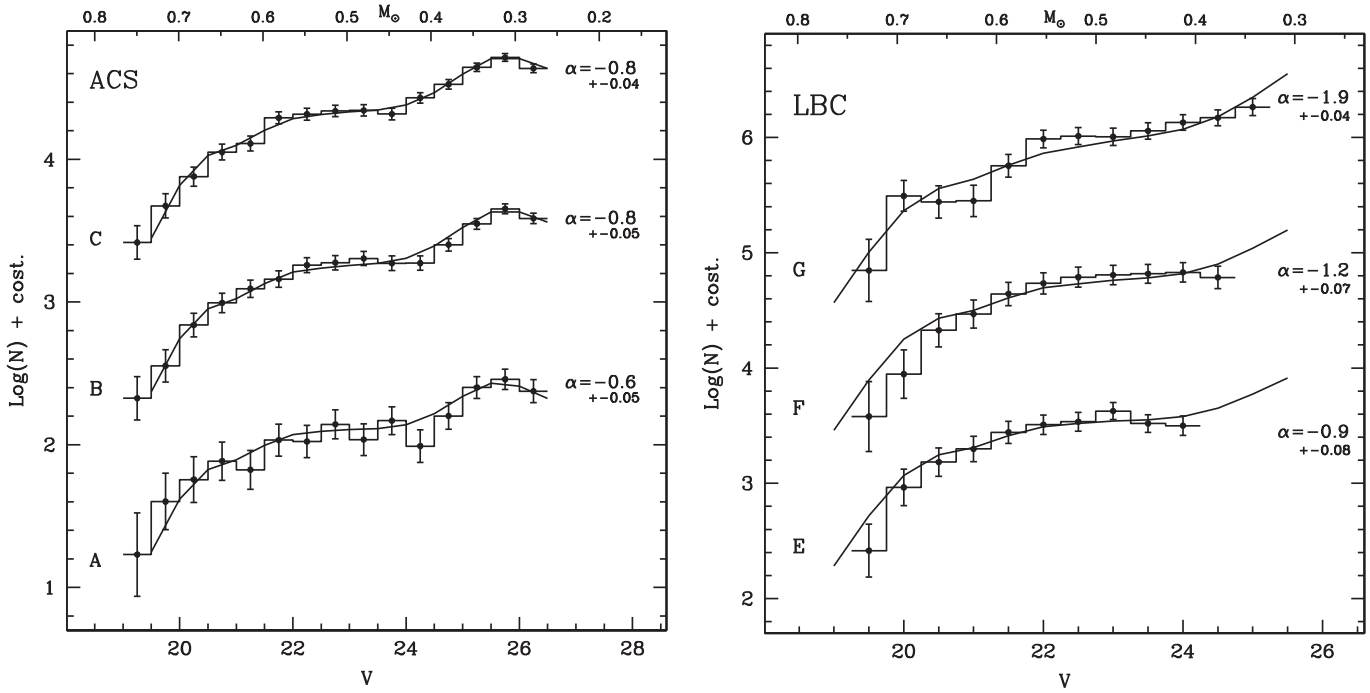

Figure 4. Observed LFs of NGC 5466, as obtained in the six radial areas (see labels) defined in Figure 3, from the ACS (left panel) and the LBC (right panel) data sets. The LFs are shifted by an arbitrary amount to make the plot more readable. The theoretical LFs that best fit the data are shown as solid lines. The corresponding power-law indexes of the MF are marked in the figure. The top axis indicates the stellar masses corresponding to the observed V magnitudes.

by stellar crowding even in the fairly loose GC-like NGC 5466. In particular, in the first radial annulus (region D), the completeness newer reaches the 100% level and it drastically drops below 50% for stellar masses $<0.5\,M_{\odot}$. We therefore decided not to include this radial bin in the study of the cluster's MF. Moreover, although the last radial bin covers a wide area, we find no significant variations in the photometric completeness and we decided to derive a unique LF in that region. We can thus assume that a single LF/MF is well representative of the entire region. Hence, the LF and MF of NGC 5466 are calculated in six areas, namely A, B, C, E, F, and G.

3. LUMINOSITY AD MASS FUNCTIONS

To derive the LF we first selected a catalog of bona fide MS stars, i.e., all stars with $V > 19$ observed within 2.5σ from the MS mean ridge line, where σ is the combined photometric uncertainty in the two bands. The sample of stars selected in this way is mostly populated by genuine single MS stars. While a fraction of binary systems will most likely contaminate the selection, these are mostly binaries characterized by low-mass ratios, whose mass (and light) budget is largely dominated by the primary star (see Sollima et al. 2007). The ACS and LBC catalogs obtained from this selection contain 19,685 and 7498 stars, respectively. The LF has been obtained by counting the number of stars with $V > 19$ in steps of 0.5 mag. The lower V-magnitude limit in each radial region corresponds to the value where the completeness is equal to 50%. A catalog of simulated stars from the Galactic model of Robin et al. (2003) has been used to take into account the contamination from field stars. We properly propagated the observer's photometric uncertainties to the simulated catalog. The completeness- and field-contamination-corrected LFs determined in the six considered areas are shown in Figure 4. The solid lines represent the theoretical LFs obtained by multiplying a simple power-law MF of the type $dN/dm \propto m^{\alpha}$ by the derivative of the mass–luminosity relationship of the best-fit isochrone (see Section 2). With such a notation, the Salpeter IMF would have a slope $\alpha = -2.35$, and a positive index implies that the number of stars decreases with decreasing mass.

The best-fit models to the observed LFs have been determined by means of a χ^2 statistical test, as the ones with the MF slopes yielding the lowest reduced-χ^2. We generated a large number of theoretical LFs using MF power-law indexes (α) ranging from -2 to 2, in steps of 0.1. The star counts in the magnitude range $20 < V < 23.5$ have been used to normalize the theoretical LFs to the observed one in each annulus, while the fit was performed down to $V = 25.5$ (i.e., $M > 0.32\,M_{\odot}$) in all cases. The choice of such a lower luminosity limit is mostly driven by the need of a compromise between sampling the largest range of stellar masses, while dealing with regions characterized by very different photometric completeness. In this sense, the best-fit models in regions E and F are partially extrapolated (in the lowest masses regime), while the LBC observations in region G (the most external one) sample a mass range that is perfectly compatible with the one covered by the ACS data.

The MF power-law indexes corresponding to the best-fit LF models for the six regions are, from the central area (A) to the most external one (G): $\alpha = -0.6, -0.8, -0.8, -0.9, -1.2, -1.9$, with uncertainties of the order of 0.05 (see labels in Figure 4). This is the first time that the LF and the MF have been determined over the entire radial extension of NGC 5466. We find that the MF slope varies only mildly from $\sim$–0.6 in the very center to -1.9 out to the cluster tidal radius.

4. DISCUSSION

As shown in the left-hand panel of Figure 4, the slope of the MF is essentially constant within the *HST* FOV (which

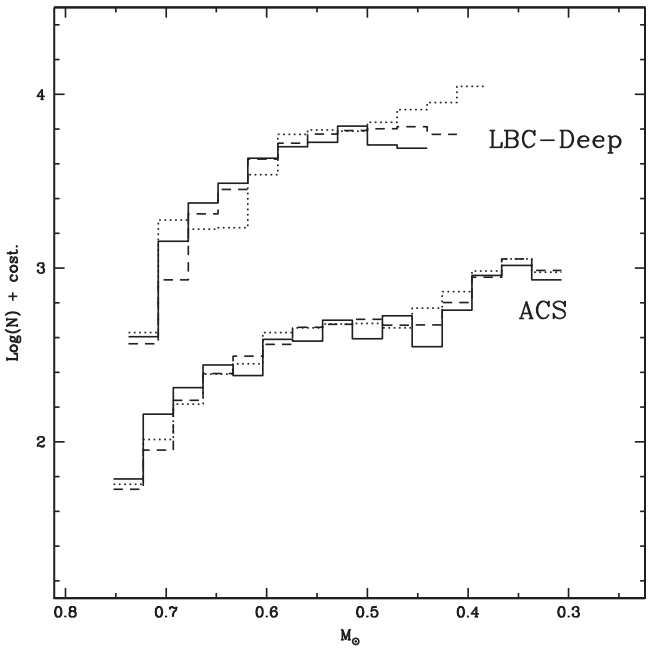

Figure 5. Direct comparison among the observed LFs in the ACS and in the LBC data sets. For both data sets, the solid line represents the most internal region, the dashed line shows the region at intermediate distance, while the dotted line is used for the one located at larger distance respect to the others in the same data set.

corresponds to almost twice the core radius, $r_c = 72''$; Miocchi et al. 2013), with only a very mild increase in the innermost region. It seems to stay constant even out to $\sim 300''$ (although the area between $120''$ and $200''$ could not be investigated with the available data sets), a distance sampled by region E, which also includes the cluster half-mass–radius ($r_{hm} = 214''$; see Miocchi et al. 2013).

Quite interestingly, the MF slope measured in region E ($\alpha = -0.9 \pm 0.08$) is in very good agreement with the value of the *global* MF[5] index predicted by the relation between α and the central concentration parameter c shown in Figure 1 of De Marchi et al. (2007). In fact, NGC 5466 has a concentration parameter $c = 1.31$ (Miocchi et al. 2013), corresponding to a global MF index $\alpha \sim -0.8$ (see Figure 1 in De Marchi et al. 2007). Such an agreement is indeed expected, since the actual MF near the half-mass radius should be only marginally affected by mass segregation and should therefore be representative of the global MF of the cluster (see De Marchi et al. 2000; Beccari et al. 2010, and references therein). On the other hand, these values are not compatible with the global MF index $\alpha = -1.15 \pm 0.03$ estimated by Paust et al. (2010), who used only ACS data and corrected the MF for the effects of mass segregation using a set of multi-mass King models.

As we move outwards, α (slowly) decreases. This can be also appreciated in Figure 5, where the LF measured in the different regions of the ACS and the LBC FOVs are overplotted. In the areas sampled by the ACS data (A, B, and C), the shape of the LF is the same, while in the regions covered by the LBC observations (E, F, and G) the most external LF (dotted line) shows an excess in the star counts at the low-mass end, with respect to the LFs measured in the other two regions (solid and dashed lines). Such a behavior in the most external bin is in agreement with that expected for a cluster moderately affected by mass segregation.

The conclusion in favor of a cluster not heavily affected by dynamical evolution (i.e., a dynamically young system) is also supported by the comparison with the results that we obtained from a similar analysis performed in the GC M10. In Beccari et al. (2010) we studied the radial distribution of the MF slope of M10 in the same mass range considered here, and out to five times the cluster core radius ($r_c = 41''$, or $2r_{hm}$ Miocchi et al. 2013). We found that, from the center out to $5r_c$, the MF index varies as: $\alpha = 0.7, 0.4, 0.1, -0.3, -0.6, -0.9$. Hence, the gradient of α in M10, defined as the absolute value of difference between its central value and the one at $5r_c$, is $\Delta\alpha_{5r_c} = 1.6$. In the case of NGC 5466, the same quantity can be calculated as the difference between the value of α in region A ($\alpha = -0.6$,) and that measured in region F ($\alpha = -1.2$), which includes the $r = 5 \times r_c$ (approximately $2r_{hm}$) distance from the cluster center. Hence, in the case of NGC 5466 we obtain $\Delta\alpha_{5r_c} = 0.6$, meaning that the variation of the MF slope is more than a factor of 2 shallower in NGC 5466 than in M10. Such a comparison indicates that two-body relaxation processes worked more efficiently in shaping the mass distribution of MS stars in M10, with respect to what happened in NGC 5466.

Note that the two clusters have quite different concentrations and global MF (Beccari et al. 2010; Miocchi et al. 2013). So, it is possible that this difference is reflected in the observed $\Delta\alpha$ variation. To test this possibility, for both clusters we fit the surface brightness and the MF in the radial bin containing the half-mass radius (where the MF slope should resemble the actual slope of the global MF) using a set of multi-mass King–Michie models (Gunn & Griffin 1979). These models have been constructed assuming eight mass bins ranging from 0.1 $M_\odot$ to the mass at the Red Giant Branch (RGB) tip and standard assumptions on the fraction of remnants (see Sollima et al. 2012). The theoretical MF slopes have been then estimated in the same radial bins adopted in the observations and are shown in Figure 6 (open squares) together with the observed ones (solid circles). While the observed variation of α in M10 (gray solid circles) is slightly steeper than what predicted by models (gray open squares), the opposite happens for NGC 5466 which appears to be under-segregated with respect to the best-fit model in the same radial range. It is important to remark here that, according to Milone et al. (2012), the core binary fraction in NGC 5466 is $\sim$14%, while it is only $\sim$8% in M10. In Beccari et al. (2010), through a set of realistic *N*-body simulations, we showed that binaries play a non-negligible role in the dynamical evolution of the cluster, acting as the energy source that quenches the effect of mass segregation in a cluster. Hence, the difference in the binary fraction in the two clusters can be at the origin (at least partially) of the different behaviors between the observed and the predicted radial distribution profiles of α. Nonetheless, the models shown in Figure 6 account for the different concentrations and MFs, since the same recipe for mass segregation is adopted. Hence the opposite systematic deviations that the observed data show with respect to the predicted behaviors indicate an actual difference in the efficiency of mass segregation which appears to be stronger in M10 than in NGC 5466.

This result is not a surprise per se. In fact, adopting the cluster's structural parameter from Miocchi et al. (2013) and

[5] Following De Marchi et al. (2000), we define the global MF as the present-day mass distribution of all cluster stars resulting from stellar evolution only, neglecting any variations due to the dynamical evolution of the system.

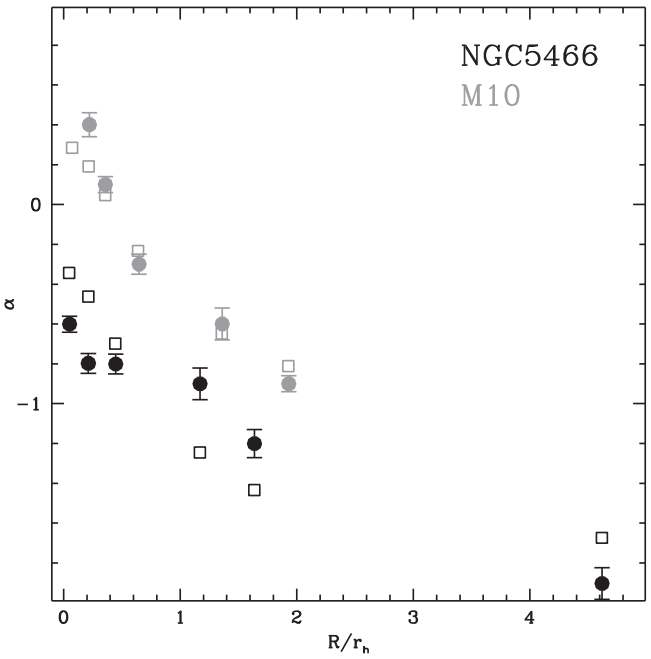

Figure 6. Radial distribution of the observed slope α of the MFs for NGC 5466 and M10 (black and gray solid circles) with respect to the theoretical ones obtained in the same radial regions (open squares) by using a set of multi-mass King–Michie models. The uncertainties on the observed values of α are also shown.

Equations (10) and (11) from Djorgovski (1993), we calculate the clusters' core and half-mass relaxation times (t_{rc} and t_{rh}) to be 2.6 and 19.9 Gyr for NGC 5466, and 0.3 and 1.9 Gyr for M10, respectively. Hence, the comparison of the expected evolutionary timescales already suggests that NGC 5466 should be dynamically younger than M10. The study proposed in this paper offers a new observational proof of the different dynamical states of the two clusters.

Very interestingly, the same conclusion is also obtained from the study of the radial distribution of BSSs and binary systems (see Paper I for NGC 5466, and Dalessandro et al. 2011, 2013 for M10). In particular, Ferraro et al. (2012) showed that the radial distribution of BSSs, normalized to that of a "normal" stellar population taken as a proxy of the distribution of the cluster's stars, is an efficient tracer of the dynamical evolution of the hosting cluster. In fact, the position of the minimum (r_{min}) of the BSS radial distribution marks the distance at which dynamical friction has already been effective in segregating BSSs toward the cluster center. Through the comparison among the values of r_{min} measured in several Galactic GCs, Ferraro et al. (2012) defined the so-called "dynamical clock," an empirical tool able to rank GCs according to their dynamical age. In this context, in Paper I we have shown that r_{min} is $\sim 2.5 r_c$ in NGC 5466, while it corresponds to $\sim 10 r_c$ in M10 (Dalessandro et al. 2013). According to the dynamical clock, NGC 5466 is therefore classified as an "early Family II" GC, while M10 is ranked in the "evolved Family II" sub-class, where dynamical friction has been more effective in shaping the radial distribution of BSSs.

All three different and independent dynamical indicators studied so far (namely, the radial trend of the MF slope presented in this work, and the radial distributions of BSSs and binaries studied in Paper I) therefore agree in showing that NGC 5466 is a GC that just started to evolve dynamically.

We wish to thank the anonymous referee for insightful comments that have helped to improve the presentation of our work. This research is part of the project COSMIC-LAB funded by the European Research Council (under contract ERC-2010-AdG-267675). This research used the facilities of the Italian Center for Astronomical Archive (IA2) operated by INAF at the Astronomical Observatory of Trieste. Also based on observations made with the NASA/ESA *Hubble Space Telescope*, obtained from the data archive at the Space Telescope Institute. STScI is operated by the association of Universities for Research in Astronomy, Inc. under the NASA contract NAS 5-26555.

REFERENCES

Albrow, M. D., De Marchi, G., & Sahu, K. C. 2002, ApJ, 579, 660
Andreuzzi, G., Testa, V., Marconi, G., et al. 2004, A&A, 425, 509
Beccari, G., Dalessandro, E., Lanzoni, B., et al. 2013, ApJ, 776, 60 (Paper 1)
Beccari, G., Ferraro, F. R., Possenti, A., et al. 2006, AJ, 131, 2551
Beccari, G., Pasquato, M., De Marchi, G., et al. 2010, ApJ, 713, 194
Beccari, G., Sollima, A., Ferraro, F. R., et al. 2011, ApJL, 737, L3
Bellazzini, M., Dalessandro, E., Sollima, A., & Ibata, R. 2012, MNRAS, 423, 844
Bellazzini, M., Fusi Pecci, F., Messineo, M., Monaco, L., & Rood, R. T. 2002, AJ, 123, 1509
Da Costa, G. S. 1982, AJ, 87, 990
Dalessandro, E., Ferraro, F. R., Lanzoni, B., et al. 2013, ApJ, 770, 45
Dalessandro, E., Ferraro, F. R., Massari, D., et al. 2015, arXiv:1507.04776
Dalessandro, E., Lanzoni, B., Beccari, G., et al. 2011, ApJ, 743, 11
Dalessandro, E., Lanzoni, B., Ferraro, F. R., et al. 2008, ApJ, 681, 311
De Marchi, G., Paresce, F., & Pulone, L. 2000, ApJ, 530, 342
De Marchi, G., Paresce, F., & Pulone, L. 2007, ApJL, 656, L65
Dieball, A., Knigge, C., Zurek, D. R., Shara, M. M., & Long, K. S. 2005, ApJ, 625, 156
Djorgovski, S. 1993, in ASP Conf. Ser. 50, Structure and Dynamics of Globular Clusters, ed. S. G. Djorgovski & G. Meylan (San Francisco, CA: ASP), 373D
Dotter, A., Chaboyer, B., Jevremović, D., et al. 2007, AJ, 134, 376
Fekadu, N., Sandquist, E. L., & Bolte, M. 2007, ApJ, 663, 277
Ferraro, F. R., Lanzoni, B., Dalessandro, E., et al. 2012, Natur, 492, 393
Ferraro, F. R., Messineo, M., Fusi Pecci, F., et al. 1999, AJ, 118, 1738
Ferraro, F. R., Possenti, A., D'Amico, N., & Sabbi, E. 2001, ApJL, 561, L93
Ferraro, F. R., Sills, A., Rood, R. T., Paltrinieri, B., & Buonanno, R. 2003, ApJ, 588, 464
Ferraro, F. R., Sollima, A., Rood, R. T., et al. 2006, ApJ, 638, 433
Frank, M. J., Grebel, E. K., & K&uumlpper, A. H. W. 2014, MNRAS, 443, 815
Guhathakurta, P., Webster, Z. T., Yanny, B., Schneider, D. P., & Bahcall, J. N. 1998, AJ, 116, 1757
Gunn, J. E., & Griffin, R. F. 1979, AJ, 84, 752
Heggie, D., & Hut, P. 2003, in The Gravitational Million-Body Problem: A Multidisciplinary Approach to Star Cluster Dynamics, ed. D. Heggie & P. Hut (Cambridge: Cambridge Univ. Press), 372
Heinke, C. O., Wijnands, R., Cohn, H. N., et al. 2006, ApJ, 651, 1098
Koch, A., Grebel, E. K., Odenkirchen, M., Martínez-Delgado, D., & Caldwell, J. A. R. 2004, AJ, 128, 2274
Lee, K. H., Lee, H. M., Fahlman, G. G., & Lee, M. G. 2003, AJ, 126, 815
Lee, K. H., Lee, H. M., Fahlman, G. G., & Sung, H. 2004, AJ, 128, 2838
Marconi, G., Andreuzzi, G., Pulone, L., et al. 2001, A&A, 380, 478
Meylan, G., & Heggie, D. C. 1997, A&ARv, 8, 1
Milone, A. P., Piotto, G., Bedin, L. R., et al. 2012, A&A, 540, A16
Miocchi, P., Lanzoni, B., Ferraro, F. R., et al. 2013, arXiv:1307.6035
Paust, N. E. Q., Reid, I. N., Piotto, G., et al. 2010, AJ, 139, 476
Robin, A. C., Reylé, C., Derrière, S., & Picaud, S. 2003, A&A, 409, 523
Rood, R. T., Carretta, E., Paltrinieri, B., et al. 1999, ApJ, 523, 752
Salinas, R., Jílková, L., Carraro, G., Catelan, M., & Amigo, P. 2012, MNRAS, 421, 960
Sirianni, M., Jee, M. J., Benítez, N., et al. 2005, PASP, 117, 1049
Sollima, A., Beccari, G., Ferraro, F. R., Fusi Pecci, F., & Sarajedini, A. 2007, MNRAS, 380, 781
Sollima, A., Bellazzini, M., & Lee, J.-W. 2012, ApJ, 755, 156
Spitzer, L. 1987, (Princeton, NJ: Princeton Univ. Press), 191
Stetson, P. B. 1987, PASP, 99, 191
Stetson, P. B. 1994, PASP, 106, 250